

Relevance of Approximated PDF Shapes for Turbulent Combustion Modelling with Variable Equivalence Ratio

Vincent Robin¹, Arnaud Mura¹, Michel Champion¹, Pierre Plion²

¹Laboratoire de Combustion et de Détonique, UPR 9028 CNRS, Poitiers, France

²Département MFTT, Electricité de France, Chatou, France

Corresponding author, M. Champion: michel.champion@lcd.ensma.fr

Abstract

The present paper is devoted to the numerical modelling of turbulent reactive flows in situations where reactants are not ideally premixed. In this case, the description of the local thermochemistry requires at least two variables. Here, we chose the mixture fraction ξ to describe the local composition of fresh mixture and the fuel mass fraction Y_f to evaluate the progress of the chemical reaction. The numerical model is based on the earlier analysis made by Libby and Williams (2000) that led eventually to the LW-P model (Ribert et al. 2004). A two-scalar (Y_f, ξ) Probability Density Function (PDF) made of two or four Dirac delta functions is used to evaluate the mean chemical rate. In the LW-P model, the parameters of the PDF describing the magnitudes and locations of these Dirac delta functions are determined solely from the mean and variance of the two variables. The model is applied to the calculation of a turbulent reactive flow of propane and air stabilized by a plane sudden expansion of a 2-D channel (Besson et al. 2001). The reaction zone is fed by two streams with different equivalence ratio (Fig.1). In the present work, the results obtained using either a two Dirac delta functions PDF or a four Dirac delta functions PDF are compared.

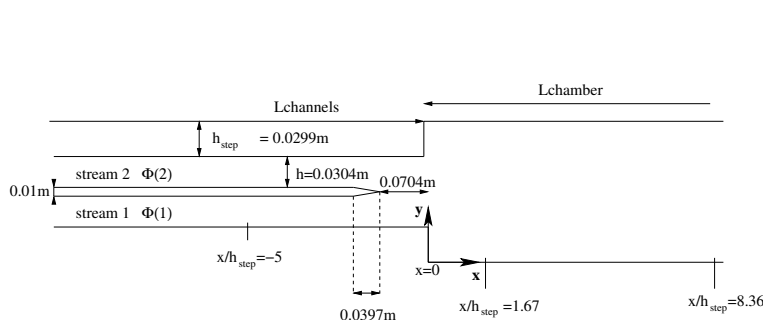


Figure 1: Experimental configuration

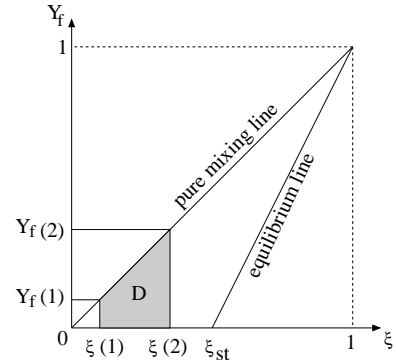


Figure 2: Domain D in the composition space

Description of the LW-P model

A normalized mixture fraction is defined as: $\xi = (Y_{N_2} - Y_{N_2}^{min}) / (Y_{N_2}^{max} - Y_{N_2}^{min})$ where indices *min* and *max* correspond to pure air and fuel respectively. It must be noticed that in the specific case investigated here these two limits are never reached and ξ stays in the range $\xi(1) \leq \xi \leq \xi(2)$. The extreme situation where $0 \leq \xi \leq 1$ would correspond to a diffusion flame.

The mass-weighted joint PDF of ξ and Y_f is first assumed to be made of two Dirac delta functions:

$$\tilde{P}(\xi, Y_f) = \alpha \delta(Y_f - Y_{f1}) \delta(\xi - \xi_1) + (1 - \alpha) \delta(Y_f - Y_{f2}) \delta(\xi - \xi_2) \quad (1)$$

A four Dirac delta functions PDF will be also considered:

$$\tilde{P}(\xi, Y_f) = \alpha \tilde{P}_1(Y_f) \delta(\xi - \xi_1) + (1 - \alpha) \tilde{P}_2(Y_f) \delta(\xi - \xi_2) \quad (2)$$

where \tilde{P}_1 and \tilde{P}_2 are the two conditional PDF at $\xi = \xi_1$ and $\xi = \xi_2$ respectively, defined as:

$$\begin{aligned} \tilde{P}_1 &= \beta \delta(Y_f - Y_{f11}) + (1 - \beta) \delta(Y_f - Y_{f12}) \\ \tilde{P}_2 &= \gamma \delta(Y_f - Y_{f21}) + (1 - \gamma) \delta(Y_f - Y_{f22}) \end{aligned} \quad (3)$$

Consequently, the mean consumption rate of fuel Y_f is defined through the following integral

$$\bar{\omega} = \bar{\rho} \int \int_D \frac{\omega(\xi, Y_f)}{\rho(\xi, Y_f)} \tilde{P}(\xi, Y_f) d\xi dY_f \quad (4)$$

D is the domain where \tilde{P} is defined.

A single step Arrhénius law for the instantaneous rate of fuel consumption is used and, Eq.(1) simply leads to the following expression for the mean reaction rate:

$$\bar{\omega} = \bar{\rho} Da \left[\begin{array}{l} \alpha \quad Y_{f1} Y_{O_2}(\xi_1, Y_{f1}) \exp(-T_a/T(\xi_1, Y_{f1})) \\ + \quad (1 - \alpha) \quad Y_{f2} Y_{O_2}(\xi_2, Y_{f2}) \exp(-T_a/T(\xi_2, Y_{f2})) \end{array} \right] \quad (5)$$

Whereas using Eq.(2) and Eq.(3), it leads to:

$$\bar{\omega} = \bar{\rho} Da \left[\begin{array}{l} \alpha \quad \left(\begin{array}{l} \beta \quad Y_{f11} Y_{O_2}(\xi_1, Y_{f11}) \exp(-T_a/T(\xi_1, Y_{f11})) \\ + \quad (1 - \beta) \quad Y_{f12} Y_{O_2}(\xi_1, Y_{f12}) \exp(-T_a/T(\xi_1, Y_{f12})) \end{array} \right) \\ + \quad (1 - \alpha) \quad \left(\begin{array}{l} \gamma \quad Y_{f21} Y_{O_2}(\xi_2, Y_{f21}) \exp(-T_a/T(\xi_2, Y_{f21})) \\ + \quad (1 - \gamma) \quad Y_{f22} Y_{O_2}(\xi_2, Y_{f22}) \exp(-T_a/T(\xi_2, Y_{f22})) \end{array} \right) \end{array} \right] \quad (6)$$

where $Da = U_0 B/d$. U_0 and d are respectively the flow characteristic velocity and length scales and B is the pre-exponential factor.

- Expressions for the parameters of a two Dirac delta functions PDF

Once modelled equations for mean and variance of ξ and Y_f have been derived and considering Eq.(1), it can be easily shown that both sets of values (ξ_1, Y_{f1}) and (ξ_2, Y_{f2}) are located on the straight lines defined by $(\xi - \tilde{\xi}) / (Y_f - \tilde{Y}_f) = \pm p$, $p = \sqrt{\rho \xi''^2 / \rho Y_f''^2}$ being the corresponding slope. If no combustion takes place, the sign of the slope must be the sign of the pure mixing line,

see Fig.(2).

Accordingly, taking into account this latter point, the positive slope must be retained in the situation depicted in Fig.(1) and the positions of the two Dirac delta functions are given by:

$$\begin{aligned}\xi_1 &= \tilde{\xi} - \sqrt{\frac{(1-\alpha)}{\alpha} \cdot \overline{(\rho\xi''^2)}/\bar{\rho}} & Y_{f1} &= \tilde{Y}_f - \sqrt{\frac{(1-\alpha)}{\alpha} \cdot \overline{(\rho Y_f''^2)}/\bar{\rho}} \\ \xi_2 &= \tilde{\xi} + \sqrt{\frac{\alpha}{(1-\alpha)} \cdot \overline{(\rho\xi''^2)}/\bar{\rho}} & Y_{f2} &= \tilde{Y}_f + \sqrt{\frac{\alpha}{(1-\alpha)} \cdot \overline{(\rho Y_f''^2)}/\bar{\rho}}\end{aligned}\quad (7)$$

Introducing a curvilinear coordinate g on the straight line, this yields the following positions for the delta functions:

$$g_1 = \tilde{g} - \sqrt{\frac{(1-\alpha)}{\alpha} \cdot \overline{(\rho g''^2)}/\bar{\rho}} \quad g_2 = \tilde{g} + \sqrt{\frac{\alpha}{(1-\alpha)} \cdot \overline{(\rho g''^2)}/\bar{\rho}} \quad (8)$$

A complementary assumption is needed to determine the magnitude α for the two delta functions PDF. Ribert et al. (2004) propose to consider that the variation about the mean is given by the variance only, so that:

$$\alpha = \frac{g^{max} - \tilde{g}}{g^{max} - g^{min}} \quad (9)$$

where g^{max} and g^{min} are respectively maximum and minimum values of g in the domain D . It should be noticed that $\tilde{g} = 0$ and $\overline{\rho g''^2} = \overline{\rho\xi''^2} + \overline{\rho Y_f''^2}$.

- Expressions for the parameters in the case of a four Dirac delta functions PDF

In this case, a additional closed balance equation for the cross correlation $\overline{\rho\xi''Y_f''}/\bar{\rho}$ must be solved.

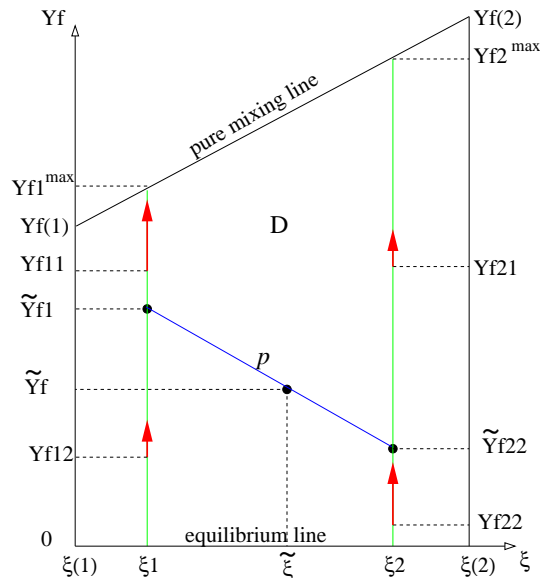


Figure 3: Locations of the four delta functions in the domain D

Two steps are then necessary to determine the PDF from Eq.(2).

- ξ_1 and ξ_2 are first determined by using:

$$\xi_1 = \tilde{\xi} - \sqrt{\frac{(1-\alpha)}{\alpha} \cdot \overline{(\rho\xi''^2)}/\bar{\rho}} \quad \xi_2 = \tilde{\xi} + \sqrt{\frac{\alpha}{(1-\alpha)} \cdot \overline{(\rho\xi''^2)}/\bar{\rho}}$$

- Then, on each line $\xi = \xi_1$ and $\xi = \xi_2$ in the plane (Y_f, ξ) , the two Dirac delta functions are determined by using conditional mean and fluctuating intensity of Y_f at ξ_1 and ξ_2 : \tilde{Y}_{f1} , $\overline{(\rho Y_{f1}''^2)/\bar{\rho}}$, \tilde{Y}_{f2} , $\overline{(\rho Y_{f2}''^2)/\bar{\rho}}$, leading to:

$$\begin{aligned} Y_{f11} &= \tilde{Y}_{f1} - \sqrt{\frac{(1-\beta)}{\beta} \cdot \overline{(\rho Y_{f1}''^2)}/\bar{\rho}} & Y_{f21} &= \tilde{Y}_{f2} - \sqrt{\frac{(1-\gamma)}{\gamma} \cdot \overline{(\rho Y_{f2}''^2)}/\bar{\rho}} \\ Y_{f12} &= \tilde{Y}_{f1} + \sqrt{\frac{\beta}{(1-\beta)} \cdot \overline{(\rho Y_{f1}''^2)}/\bar{\rho}} & Y_{f22} &= \tilde{Y}_{f2} + \sqrt{\frac{\gamma}{(1-\gamma)} \cdot \overline{(\rho Y_{f2}''^2)}/\bar{\rho}} \end{aligned} \quad (10)$$

Four additional equations are required to set the values of the four still unknown quantities: \tilde{Y}_{f1} , $\overline{(\rho Y_{f1}''^2)/\bar{\rho}}$, \tilde{Y}_{f2} , $\overline{(\rho Y_{f2}''^2)/\bar{\rho}}$.

Among them, three equations are obtained by expressing the mean value, the intensity and the cross correlation:

$$\begin{aligned} \tilde{Y}_f &= \alpha \tilde{Y}_{f1} + (1-\alpha) \tilde{Y}_{f2} \\ \overline{(\rho Y_f''^2)/\bar{\rho}} + \tilde{Y}_f^2 &= \alpha \left(\tilde{Y}_{f1}^2 + \overline{(\rho Y_{f1}''^2)/\bar{\rho}} \right) + (1-\alpha) \left(\tilde{Y}_{f2}^2 + \overline{(\rho Y_{f2}''^2)/\bar{\rho}} \right) \\ \overline{(\rho \xi'' Y_f'')/\bar{\rho}} + \tilde{\xi} \tilde{Y}_f &= \alpha \xi_1 \tilde{Y}_{f1} + (1-\alpha) \xi_2 \tilde{Y}_{f2} \end{aligned} \quad (11)$$

Then an additional closure assumption is obtained by stating that the conditional normalized fluctuations intensities at ξ_1 and ξ_2 are the same:

$$\overline{(\rho Y_{f1}''^2)/\bar{\rho}} / \left[\left(Y_{f1}^{max} - \tilde{Y}_{f1} \right) \left(\tilde{Y}_{f1} - Y_{f1}^{min} \right) \right] = \overline{(\rho Y_{f2}''^2)/\bar{\rho}} / \left[\left(Y_{f2}^{max} - \tilde{Y}_{f2} \right) \left(\tilde{Y}_{f2} - Y_{f2}^{min} \right) \right] \quad (12)$$

where Y_{fi}^{min} and Y_{fi}^{max} ($i = 1, 2$) are the values at the boundaries of the domain D on equilibrium and pure mixing lines respectively, see Fig.(3).

The same assumption as the one used for the two delta function model is invoked to evaluate the magnitudes of α , β and γ , so that :

$$\alpha = \frac{\xi(2) - \tilde{\xi}}{\xi(2) - \xi(1)} \quad \beta = \frac{Y_{f1}^{max} - \tilde{Y}_{f1}}{Y_{f1}^{max} - Y_{f1}^{min}} \quad \gamma = \frac{Y_{f2}^{max} - \tilde{Y}_{f2}}{Y_{f2}^{max} - Y_{f2}^{min}}$$

Within the four delta function model, it can be shown that the slope of the straight line defined by the two points (ξ_1, \tilde{Y}_{f1}) and (ξ_2, \tilde{Y}_{f2}) of the domain D is given by $p = \overline{(\rho \xi'' Y_f'')/\bar{\rho}} / \overline{(\rho \xi''^2)/\bar{\rho}}$, see Fig.(3).

Results from numerical simulations

The LW-P model is implemented in an industrial CFD code developed by EDF: *Code-Saturne* (Archambeau et al. 2004). Numerical results are compared with the experiments of Besson (2001) made on the flow geometry given by Fig.(1). Turbulent mixing is represented through a conventional one-point two-equations $k - \epsilon$ model.

- Non reactive flow field

To characterize the flow without combustion, each of the two input channels are fed with a mass flow rate of nearly 100 g/s of air. Fig.(4) shows the profiles of the mean axial velocity component \tilde{u} , the mean transversal velocity component \tilde{v} and the turbulent kinetic energy k in the input channels at $x/h_{step} = -5$. The X-coordinate $x/h_{step} = -5$ corresponds to the input boundary condition of our numerical mesh.

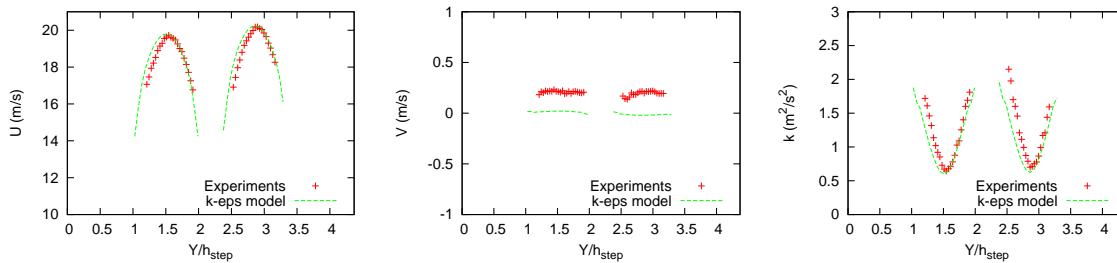


Figure 4: Mean velocity components (\tilde{u} , \tilde{v}) and turbulent kinetic energy k at $x/h_{step} = -5$

A small asymmetry between the experimental profiles of the mean axial velocity can be noticed. This slight difference between the two velocity profiles must be taken into account in these simulations. In order to apply well-defined boundary conditions, two preliminary calculations of fully developed turbulent channels have been carried out. Both calculations are identical but the mass flow rates are slightly different. A satisfactory agreement is obtained between the imposed boundary conditions and the experimental measurements provided by Besson (2001), see Fig.(4).

Fig.(5) shows the profiles of the mean velocity components (\tilde{u} , \tilde{v}) and the turbulent kinetic energy k at the location of the plane sudden expansion ($x/h_{step} = 0$) and in the combustion chamber at $x/h_{step} = 1.67$ and $x/h_{step} = 8.36$. The calculated profiles of \tilde{u} and \tilde{v} at $x/h_{step} = 0$ show a good agreement with the experimental results. Nevertheless, turbulent kinetic energy values are slightly underestimated.

The experimental and calculated velocity profiles in the combustion chamber are very similar but the lengths of the two recirculation zones are slightly underestimated. This is a well-known discrepancy due to the $k-\epsilon$ model which is not able to predict the re-attachment lengths with sufficient accuracy (Ha Minh, 1999). As a consequence of the small asymmetry existing between the two velocity profiles at $x/h_{step} = -5$, the lengths of the two recirculation zones are quite different, see Fig.(6).

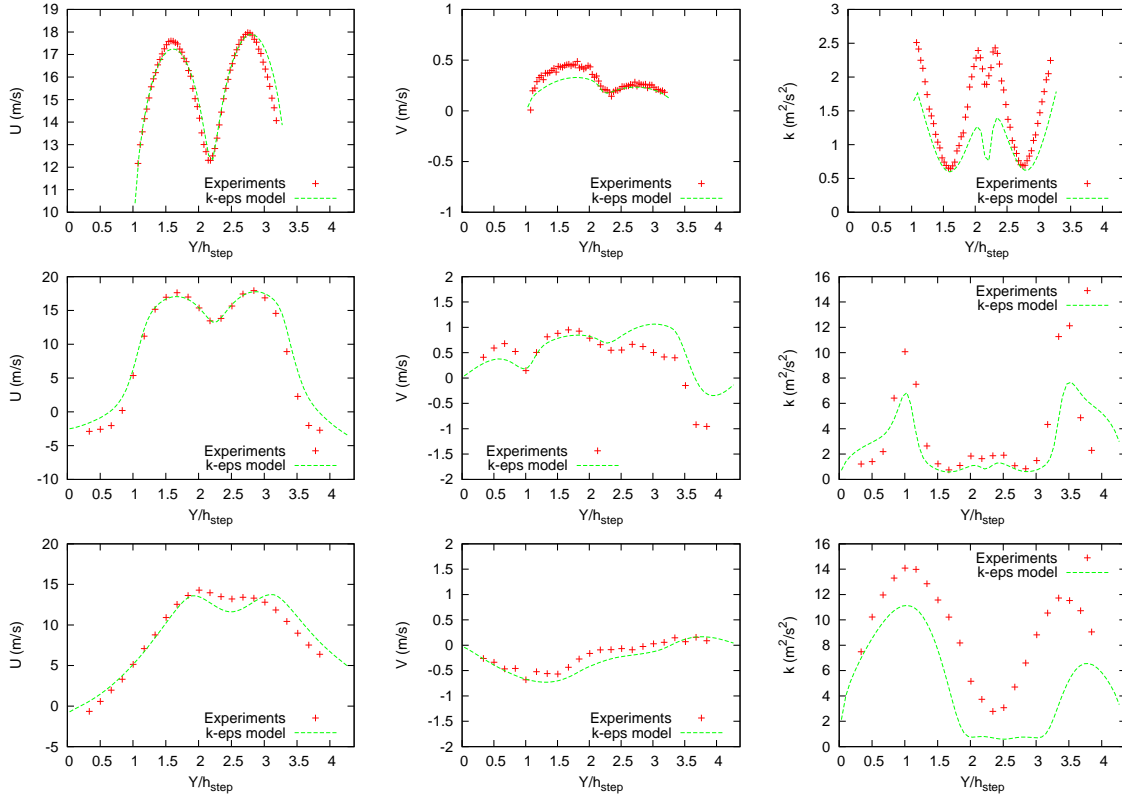


Figure 5: Mean velocity components (\tilde{u} , \tilde{v}) and turbulent kinetic energy k at $x/h_{step} = 0$ (first set of curves from the top), at $x/h_{step} = 1.67$ (second) and at $x/h_{step} = 8.36$ (third)

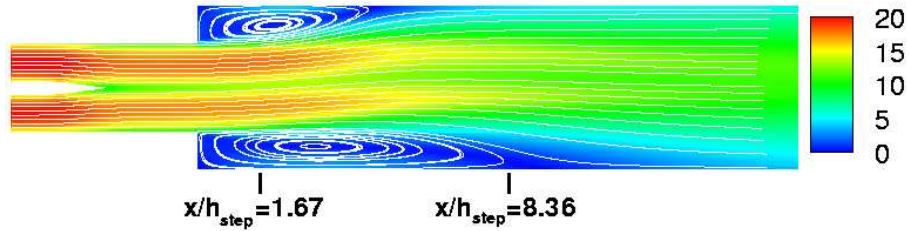


Figure 6: Velocity field (m/s) and streamlines

- Fully premixed combustion

In a first step we simulate a fully premixed turbulent flame. In this case, the two models described in the previous sections reduce to a single one.

Fig.(7) provides mean profiles in the case of mass flow rate of nearly 100 g/s of propane and air in each of the two channels. Both incoming streams have the same equivalence ratio: $\Phi(1) = \Phi(2) = 0.8$. The boundary conditions applied to the simulations are again asymmetrical. At $x/h_{step} = -5$, profiles of \tilde{u} and \tilde{v} show a good agreement with the available experimental data whereas profiles of turbulent kinetic energy are less satisfactory. Nevertheless, our calculations compare well with experimental results once the coherent part of the fluctuations is removed (Besson 2001).

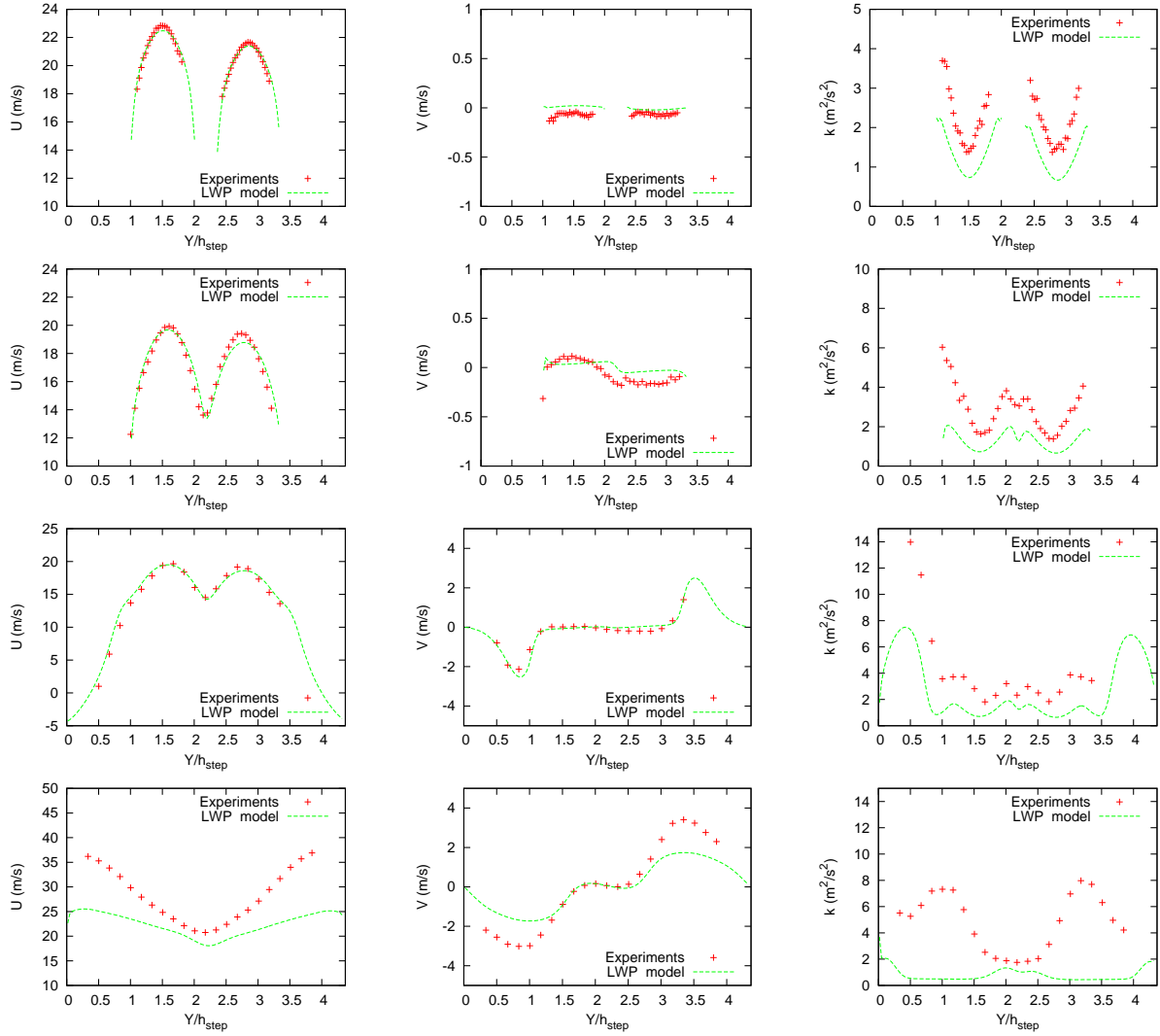


Figure 7: Mean velocity components (\tilde{u} , \tilde{v}) and turbulent kinetic energy k at $x/h_{step} = -5$ (first set of curves from the top), at $x/h_{step} = 0$ (second), at $x/h_{step} = 1.67$ (third) and at $x/h_{step} = 8.36$ (fourth)

Fig.(7) shows that the acceleration behind the flame at $x/h_{step} = 8.36$ induced by the expansion in the burned gases is found to be less important than the one existing in the experiment. This trend has been already observed in a previous calculation of the same flow, taking into account wall heat losses and the use of a detailed chemistry (Ribert et al. 2005). It must be noticed that the simple k - ϵ model used here does not contain a mechanism taking into account flame induced turbulence.

Fig.(8) compares the experimental and simulated profiles of temperature in the combustion chamber at $x/h_{step} = 1.67$ and $x/h_{step} = 8.36$. The maximum levels of temperature are higher than expected from the experiments as shown by Fig.(8). This difference can be explained when heat losses (through radiation and solid walls) as well as detailed chemistry are taken into account. However, with our present objective which is to investigate partially premixed situations, the use of complex

chemistry is not envisaged.

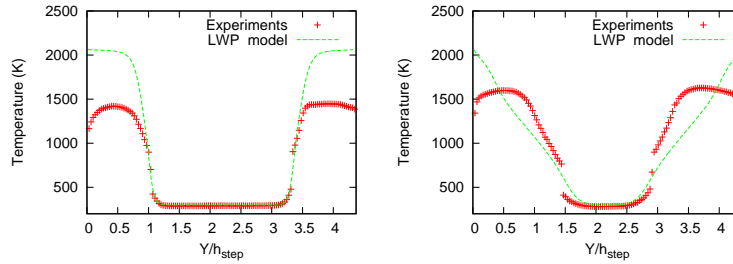


Figure 8: Mean temperature at $x/h_{step} = 1.67$ and $x/h_{step} = 8.36$

Moreover, locations of the maximum temperature gradient as well as the flame brush positioning in flow field are well recovered with this version of LW-P model based on a single step chemistry, see Fig.(9).

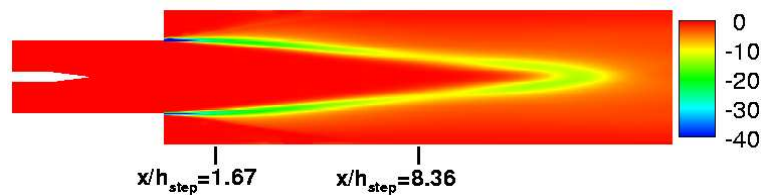


Figure 9: Mean chemical rate (s^{-1})

-Partially premixed combustion

The equivalence ratios of the two feeding streams are now considered as different. Two cases are investigated, in the first one: $\Phi(1) = 0.3$, $\Phi(2) = 0.9$, and in the second: $\Phi(1) = 0.7$ and $\Phi(2) = 0.9$. In fact, fields of the mean reaction rate presented in Fig.(10) are obtained by using the four delta function PDF. The fields obtained with the two delta PDF are found to be similar in the regions where there is no interaction between the flame and the mixing layer. Results do show that, the greater is the difference between the equivalence ratios of the two feeding streams, the more asymmetrical is the mean flow, and the mixing layer thickness becomes larger (white line). In the first case, the equivalence ratio $\Phi(1) = 0.3$ is even too low to lead to ignition.

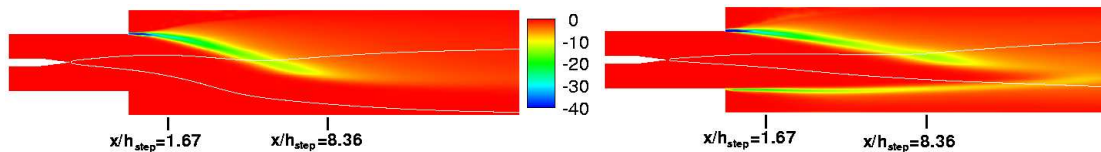


Figure 10: Mean chemical rate (s^{-1}). Left: $\Phi(1)=0.3$, $\Phi(2)=0.9$. Right: $\Phi(1)=0.7$, $\Phi(2)=0.9$

Fig.(11) shows the profiles of \tilde{u} , \tilde{v} and k at $x/h_{step} = 1.67$ and $x/h_{step} = 8.36$. The acceleration in the burned gases is more important for the higher equivalence ratio.

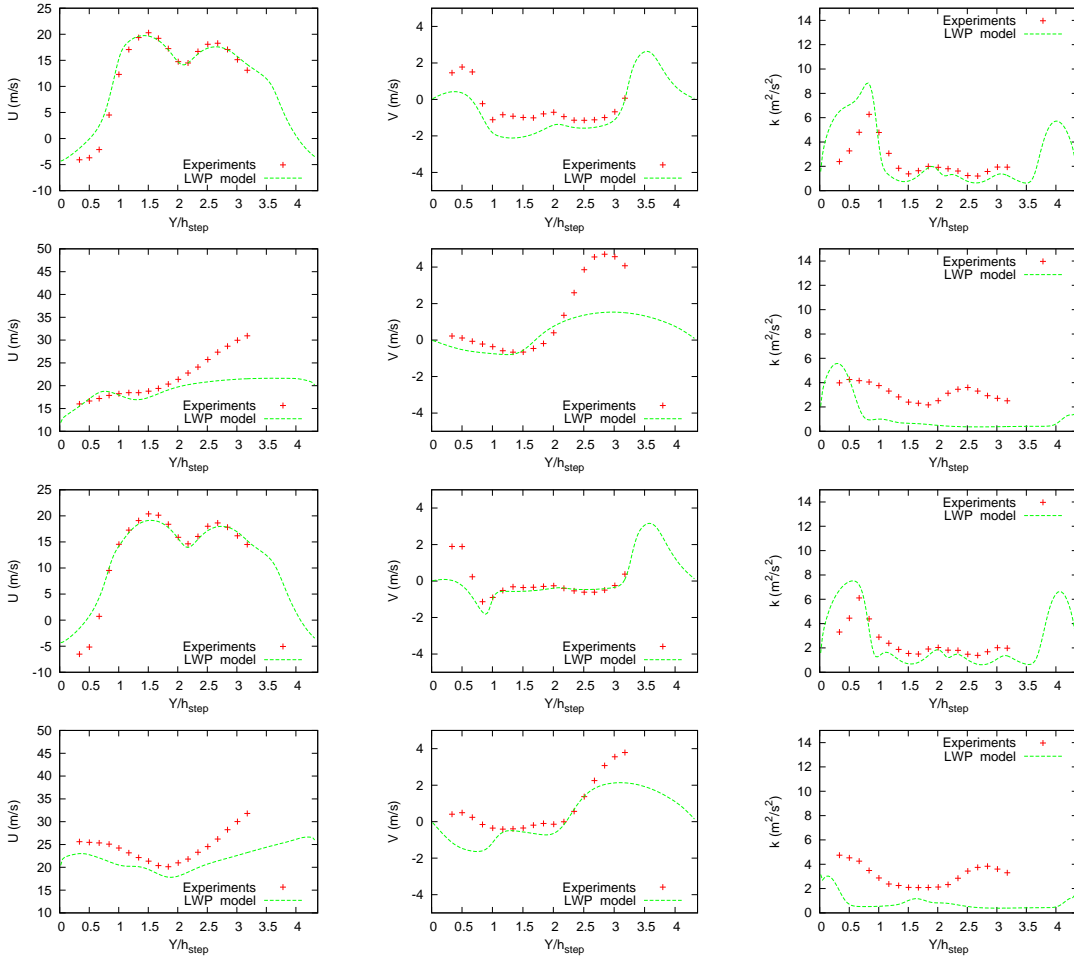


Figure 11: Mean velocity components (\tilde{u} , \tilde{v}) and turbulent kinetic energy k for $\Phi(1)=0.3$, $\Phi(2)=0.9$ at $x/h_{step}=1.67$ (first set of curves from the top) and at $x/h_{step}=8.36$ (second), for $\Phi(1)=0.7$, $\Phi(2)=0.9$ at $x/h_{step}=1.67$ (third) and at $x/h_{step}=8.36$ (fourth)

The relevance of each of these two forms for the PDF, depending on the value of the fuel air ratio, can be investigated by looking at the cross correlation $\overline{\rho\xi''Y_f''}/\overline{\rho}$. When the two delta PDF is used, this correlation is given by:

$$\overline{\rho\xi''Y_f''} = \sqrt{\overline{\rho\xi''^2} \cdot \overline{\rho Y_f''^2}}$$

in such a manner that:

$$G = \overline{\rho\xi''Y_f''} / \sqrt{\overline{\rho\xi''^2} \cdot \overline{\rho Y_f''^2}} = 1 \quad (13)$$

whereas when the four delta PDF is used, this cross correlation is determined through a modelled transport equation. Figure (12) provides the result obtained when using the four delta functions PDF. Clearly this ratio is found to be different from unity in the region where the flame and the mixing layer interact. The sign of G is even found to change when crossing the flame. The value of the correlation ($\overline{\rho\xi''Y_f''}/\overline{\rho}$) and the corresponding sign of the slope p , defined in the previous

sections of the paper, result from the competition between mixing and chemical reaction within the domain of definition of the PDF. For sufficiently lean mixtures, in the vicinity of $\xi(1)$, fluctuations of ξ around the mean values are expected to be essentially positive whatever is the value of Y_f and the cross correlation is likely to be mainly driven by the mixing mechanism. This results in positive values of $(\overline{\rho\xi''Y_f''}/\bar{\rho})$ observed in the lower stream of the mixing layer. On the contrary, the correlation $(\overline{\rho\xi''Y_f''}/\bar{\rho})$ is more likely to be driven by chemical processes for near stoichiometric conditions $\xi(2)$ resulting in the negative slope p sketched in Fig.(13). Consequently, the PDF made of two Dirac delta functions does not seem to be adequate to describe the evolution of the PDF in the near stoichiometric conditions of region (2) because in this part of the domain of definition of the PDF, the slope or conversely the cross correlation is likely to be negative as sketched in Fig.(13).

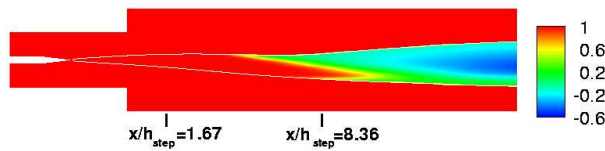


Figure 12: Normalized cross correlation G

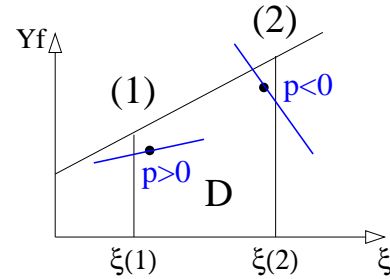


Figure 13: Domain of definition D

Conclusion

Finally, as expected when considering the work already done by Ribert et al. (2004), the results obtained using both the two delta and the four delta PDF are in good agreement with experimental observations. Nevertheless, results reported in the present study supports the use of a four delta PDF when significant variations in the equivalence ratio and near stoichiometric conditions are considered.

The decrease of turbulent kinetic energy in the flame is probably due to the use of a first order model ($k - \epsilon$) which does not take into account the turbulent production in the flame. A second order model should be better in particular to take into account the counter gradient diffusion effects. In this respect, the extension of the modelling approach discussed by Domingo and Bray (2001) is now in progress to deal with reactive scalar transport in such kind of partially premixed media.

References

- Archambeau F., Nehitoua N., and Sakiz M. (2004), "Code Saturne: A finite volume code for turbulent flows", *Int. J. Finite Volumes*, <http://averoes.math.univ-paris13.fr/IJFV/>
- Besson M. , Bruel P., Champion J.L. and Deshaies B. (2000), "Experimental analysis of combusting flows developing over a plane-symmetric expansion", *Journal of Thermophysics and Heat Transfer*, **14(1)**:59-67.

Besson M. (2001), "Etude expérimentale d'une zone de combustion en écoulement turbulent stabilisé en aval d'un élargissement brusque symétrique", *PhD Thesis, University of Poitiers*.

Domingo P. and Bray K.N.C. (2000), "Laminar flamelet expressions for pressure fluctuation terms in second moment models of premixed turbulent combustion", *Combustion and Flame*, **121**:555-574.

Ha Minh H. (1999), "La modélisation statistique de la turbulence: ses capacités et ses limitations", *C.R. Acad. Sci. Paris - Série IIB*, **327**:343-358.

Libby P.A. and Williams F.A. (2000), "Presumed pdf analysis of partially premixed turbulent combustion", *Combust. Sci. and Tech.*, **161**:351-390.

Ribert G., Champion M. and Plion P. (2004), "Modelling turbulent reactive flows with variable equivalence ratio : application to the calculation of a reactive shear layer", *Combust. Sci. and Tech.*, **176**:907-923.

Ribert G., Champion M. , Gicquel O., Darabiha N. and Veynante D. (2005), "Modelling nonadiabatic turbulent premixed reactive flows including tabulated chemistry", *Combustion and Flame*, **141**:271-280.